Chemical Engineering Journal 149 (2009) 35–41

Contents lists available at ScienceDirect

Chemical Engineering Journal

journal homepage: www.elsevier.com/locate/cej

Syngas production from methane oxidation using a non-thermal plasma: Experiments and kinetic modeling

Jocelyn Luche, Olivier Aubry, Ahmed Khacef, Jean-Marie Cormier*

GREMI-Polytech'Orléans, 14 rue d'Issoudun, B.P. 6744, 45067 Orléans Cedex 2, France

ARTICLE INFO

Article history:
Received 12 June 2008
Received in revised form
18 September 2008
Accepted 25 September 2008

Keywords:
Non-thermal plasma
Syngas
Methane
Partial oxidation
Kinetic modeling

ABSTRACT

The laboratory-scale behaviour of a methane–air mixture injected at atmospheric pressure and ambient temperature into a non-thermal plasma (NTP) reactor is investigated experimentally and numerically as a function of CH_4 concentration and mass flow rate. Numerical simulations of the NTP reactor gas phase are performed with a chemical kinetic model used initially for CH_4 oxidation in a perfectly stirred reactor (PSR). The computed H_2, CO, CO_2 and remaining CH_4 mole fractions are in good agreement with experimental data. Syngas (H_2 and CO) production from CH_4–air mixture is demonstrated over a large range of fuel flow rates and methane amounts in air. The lowest energy cost of H_2 production is about 45 $kWh/kg_{(H_2)}$ for the highest mass flow rate. Numerical simulation has confirmed that the optimum use of electrical power by the NTP reactor is achieved for high mass flow rates and low inlet CH_4 concentration in air.

1. Introduction

To meet the increasingly stringent environmental regulations on pollution-related problems (nitrogen oxides, greenhouse gases, fine particle matter), several scientific studies have developed alternative and renewable technologies for energy and electricity production. An extensively studied way of improving combustion processes and drastically decreasing noxious emissions is fuel–air conversion into synthetic gas (H_2 + CO), also known as syngas.

Traditionally, syngas production has been achieved by using catalytic reformers [1–6]. However, in addition to its high economic investment cost [7–11], this conventional technology presents several drawbacks. The catalyst device can be poisoned by sulfur or halogen-containing compounds [11–15] and catalyst surface performances can be reduced by solid carbon adsorption or deposition [8–12,16–18]. The treatment or maintenance required to remove the contaminated catalytic equipment can represent a major drawback with respect to current environmental regulations [7–11]. Moreover, catalytic sites need to be activated by heating at high temperature [7–10,12,13,15,16,18,19]. Another problem reported in the literature is the low flow rate of inlet gas injected into catalyst devices [15].

To overcome all these catalyst difficulties, fuel reforming by non-conventional technology such as plasma (both thermal and non-thermal) technology is being increasingly investigated. Thermal plasma, in which the electron temperature (>10,000 K) is equal to the gas temperature, has been successfully used in fuel–air mixture conversion into syngas to increase internal combustion engine efficiency and to reduce NO_x emissions [20–22]. While a previous study [22] has shown that comparable H_2 yields can be obtained with thermal and non-thermal plasmas, energy consumption is significantly lower in the case of non-thermal plasma (NTP), in which the electron temperature (>10,000 K) is higher than the gas temperature (300–3000 K) [10,11,19,23–26]. The main role of such a plasma is to provide energy for the production of reactive species (radicals, electron and ions) and to enhance fuel reforming reactions [7–30]. Thus, for approximately thirty years, NTP technologies have been successfully applied to combustion processes to produce H_2 and CO from the reforming of methane or natural gas [7–9,12,16–19,27–30], ethanol [23], propane [9,30], pentane [9], hexane [10] or gasoline [11,13,14,20,21].

The purpose of this work is to evaluate experimentally and numerically the conversion of methane–air mixture into syngas by using a laboratory-scale non-thermal plasma reactor. In the following section, the experimental devices, with parametrical conditions and chemical analyzers are briefly presented. Section 3 describes and discusses the experimental results of the CH_4/air mixture partial oxidation conditions. In this part, the energy cost of hydrogen production is systematically given as a function of the methane composition in air and mass flow rate. The numerical assumptions chosen to model the species behaviour in NTP reactor are briefly described in Section 4. Numerical mole fractions

* Corresponding author. Tel.: +33 2 38 49 46 09; fax: +33 2 38 41 71 54.
E-mail address: jean-marie.cormier@univ-orleans.fr (J.-M. Cormier).

1385-8947/$ – see front matter © 2008 Elsevier B.V. All rights reserved.
doi:10.1016/j.cej.2008.09.045

Nomenclature

$[CH_4]_0$	initial concentration of methane in air (%),
EC_{H_2}	energy cost per kg of H_2 produced ($kWh/kg_{(H_2)}$),
h_k	mass enthalpy of the kth species ($J\,g^{-1}$),
h_k^*	mass enthalpy of the kth species at inlet conditions ($J\,g^{-1}$),
$\dot{m}$	mass flow rate ($g\,s^{-1}$),
P_{ch}	chemical reaction power exchange (W),
P_{el}	electrical power corresponding to Joule heating of plasma column (W),
P_{fr}	power exchange due to enthalpy and mass flow rate variations (W),
P_{tc}	heat power losses or thermal conduction exchanges (W),
$\|Q\|$	power taking into account heat loss or heat inlet through reactor wall (W),
μ_k	molecular weight of the kth species ($g\,mol^{-1}$),
V	reaction volume (cm^3),
W_k	molar rate of production of the kth species per unit of volume ($mol\,cm^{-3}\,s^{-1}$),
Y_k	mass fraction of the kth species,
Y_k^*	mass fraction of the kth species at inlet conditions.

and power results are computed by using a chemical kinetic model usually dedicated to methane oxidation in combustion studies. Section 5 presents comparisons between numerical modeling results and experimental measurements considering H_2, CO, CO_2 and the remaining CH_4 mole fractions. The energy efficiency of the NTP system is also discussed by comparing numerical and experimental results.

2. Experimental devices

Laboratory-scale experiments were carried out with a CH_4/air mixture injected at atmospheric pressure and room temperature ($T \sim 295$ K) into a non-thermal plasma reactor (Fig. 1). The NTP reactor includes a quartz tube (400 mm length and 30 mm inner diameter) containing two electrodes made of graphite. The conical extremities of the two electrodes are placed opposite each other in the central axis of the reactor and with a 10 mm gap. The discharge column resembles a plasma string with a diameter of 2 mm diameter and length of 10 mm (Fig. 1).

Experiments are carried out with initial methane concentrations in air $[CH_4]_0$, ranging from 18 to 40% (volume). The chosen $[CH_4]_0$ are higher than the upper explosive limit (16% CH_4 in air). The upper value of 40% methane in air was chosen in order to avoid significant soot deposition on the reactor wall and to prevent the formation of a soot-bridge between the electrodes, leading to the electrical short-circuit of the system. Moreover, in our experimental conditions, small amounts of solid carbon particles or soot deposits are systematically observed on electrodes, quartz tube and sample pipes. These solid carbon deposits, which do not disrupt the experimental process, explain the deficit in total carbon amounts between the results of exhaust gas and initial methane/air mixture mole fractions.

The CH_4/air mixture is introduced into the reactor through the bottom electrode at a total mass flow rate ranging from 0.004 to 0.175 $g\,s^{-1}$. Exhaust gas is sampled through holes in the upper part of the reactor and is cooled down in order to eliminate water before chemical analysis. Dry output gas is analyzed and H_2, O_2, N_2, CO, CO_2, CH_4, C_2H_2, C_2H_4 and C_2H_6 species are quantified using a gas

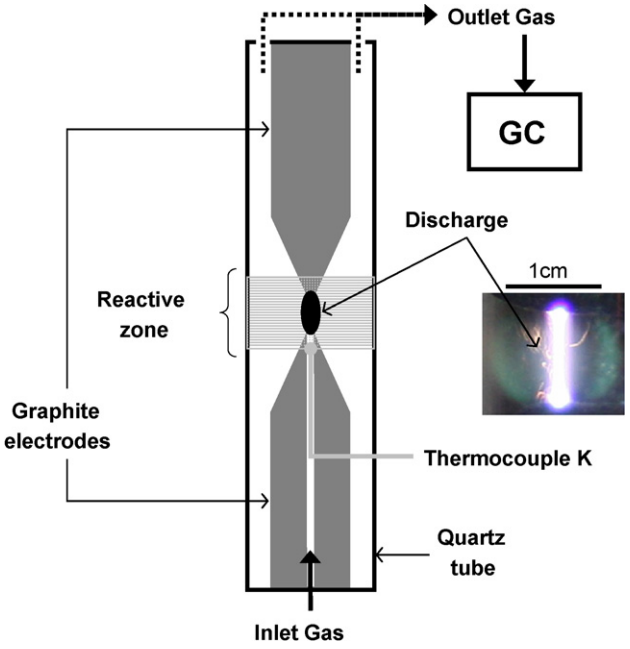

Fig. 1. Schematic representation of the plasma reactor with a photography of the electrical discharge.

phase chromatography analyzer (GC-Varian CP 3800). Two columns (5 Å Molecular Sielve and Hayesep A) are included in the GC analyzer equipped with a thermal conductivity detector (TCD) and flame ionization detector (FID), respectively. These detectors were calibrated with standards of known composition. The maximum relative deviations on mole fractions measured during calibrations are ±5%.

The mean temperature of the CH_4/air mixture before the plasma discharge is measured by a K-type thermocouple. The maximum deviation on the measured temperature is about ±20 K. Fig. 2 shows the variation in this temperature as a function of total mass flow rate. When the mass flow rate increases from 0.004 to 0.175 $g\,s^{-1}$,

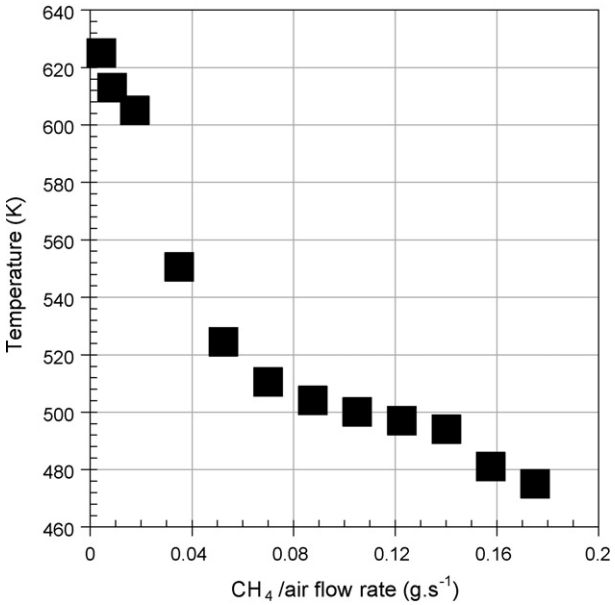

Fig. 2. Gas temperature at the inlet of reactive zone *vs.* CH_4/air mass flow rate ($[CH_4]_0 = 25\%$).

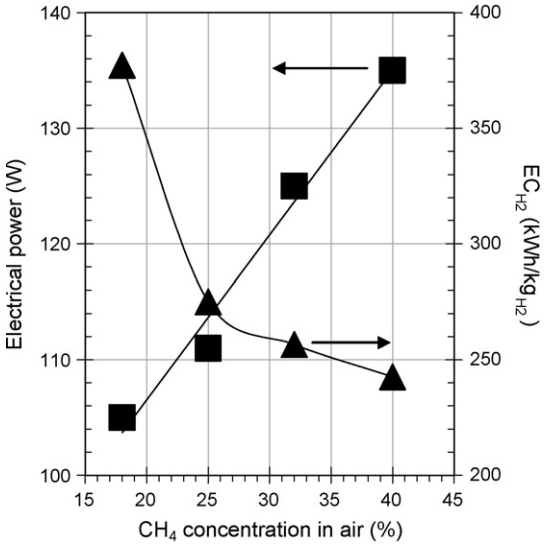

Fig. 3. P_{el} and EC_{H_2} *vs.* initial CH_4 concentration in air (mass flow rate = 0.004 g s^{-1}).

the temperature at the inlet of reactive volume decreases from 630 to 480 K, respectively.

The plasma reactor is powered by a 50 Hz high voltage (15 kV) step-up transformer with leakage flux which produces a sinusoidal current waveform with a constant root mean square value of 155 mA. The non-equilibrium (non-thermal) nature of the plasma created in these conditions has been demonstrated previously [23,30,31]. This plasma is characterized by: (i) a substantial difference between the electron temperature (>10,000 K) and gas temperature (300–3000 K), (ii) a high electrode voltage drop (>100 V), and (iii) a low current (<200 mA). The current and voltage were measured using a TCP202 Tektronix Hall effect probe and a ST500 high voltage differential probe, respectively. Signals from these probes are recorded on a Tektronix TDS 460A digital oscilloscope and processed on a PC. The mean electrical discharge power is computed from voltage–current waveforms ($P_{el} = \frac{1}{T}\int u(t)\cdot i(t)\cdot dt$) and averaged over a large number of discharges. Results are shown as a function of methane concentration and mass flow rate in the next section (Figs. 3 and 6, respectively). The mean power values are in the range 100–160 W depending on experimental conditions.

3. Experimental results and discussion

Dry outlet species analyses were carried out for the following experimental conditions:

(i) Inlet CH_4 concentration ranged from 18 to 40% (volume) in air for a total mass flow rate kept constant at about 0.004 g s^{-1},
(ii) 25% CH_4 in air for a mass flow rate ranged from 0.004 to 0.175 g s^{-1}.

3.1. CH_4 concentration effect on outlet gas concentrations

Exhaust gas mole fractions (symbols) are shown in Fig. 4 as a function of the initial concentration of CH_4 in Air. As $[CH_4]_0$ increases from 18 to 40%, the H_2 mole fraction increases from 0.19 to 0.39 and the CH_4 mole fraction from 0.01 to 0.06, respectively. The CO mole fraction increases slightly from 0.13 to 0.15 while the CO_2 mole fraction decreases from 0.03 to 0.00. In these experiments, C_3 and C_4 hydrocarbon concentrations measured on a GC analyzer are below 20 ppm and can be considered as negligible compared to C_2H_2, C_2H_4 and C_2H_6 concentrations. Indeed, C_2 species mole fractions increase with increasing $[CH_4]_0$ and always stay below 0.02. These results suggest that initial CH_4 is mainly consumed to produce syngas ($H_2 + CO$) by partial oxidation (POX) reaction ($CH_4 + 1/2O_2 \rightarrow CO + 2H_2$).

Fig. 3 gives electrical power (P_{el}) and energy cost of H_2 production (EC_{H_2}) as a function of initial CH_4 concentration in air. EC_{H_2} is computed from the following expression: $EC_{H_2} = P_{el}/(3600 \cdot D_{H_2})$, where D_{H_2} is the mass flow rate of dry H_2 produced and P_{el} the reactor discharge power. In the experimental device, the mass flow rate of exhaust gas is 1.13 (±0.03) times the initial mass flow rate. P_{el} increases from 105 to 135 W and EC_{H_2} decreases from 380 to 240 kWh/kg$_{(H_2)}$ for an increase of $[CH_4]_0$ from 18 to 40%, respectively. These results show that for the highest CH_4 amount in air, H_2 mole fraction and P_{el} are maximum (0.4 and 130 W, respectively) corresponding to the lowest EC_{H_2} value (~ 240 kWh/kg$_{(H_2)}$).

3.2. CH_4/air mixture flow rate effect on outlet gas concentrations

Fig. 5 shows outlet gas mole fractions (symbols) as a function of CH_4/air mass flow rate. It can be seen that the H_2 mole fraction decreases from 0.29 to 0.05 and the CO mole fraction from 0.17 to 0.03. Furthermore, the remaining CH_4 mole fraction increases from 0.02 to 0.20, while the CO_2 and C_2 mole fractions stay in all cases below 0.01. No significant amount of species heavier than C_2-hydrocarbons was observed in these experiments.

Results suggest that CH_4 conversion by POX reaction into syngas is enhanced by a low CH_4/air mass flow rate. In these experimental conditions, the residence time in the plasma reactor increases, promoting the production of active species and thus enhancing the methane partial oxidation into syngas. The discharge occurs as a column between the conical extremities of the two electrodes in the axis of the plasma reactor (Fig. 1). When the mass flow rate increases, the velocity of the CH_4/air mixture exiting the bottom electrode increases, causing an increase in plasma discharge length. At high mass flow rate, the plasma discharge moves away from the axis of the reactor towards the quartz tube wall where the gap is much higher than 10 mm. In that case, only part of the CH_4/air mixture is treated by the discharge, leading to the low production of H_2 by POX reaction.

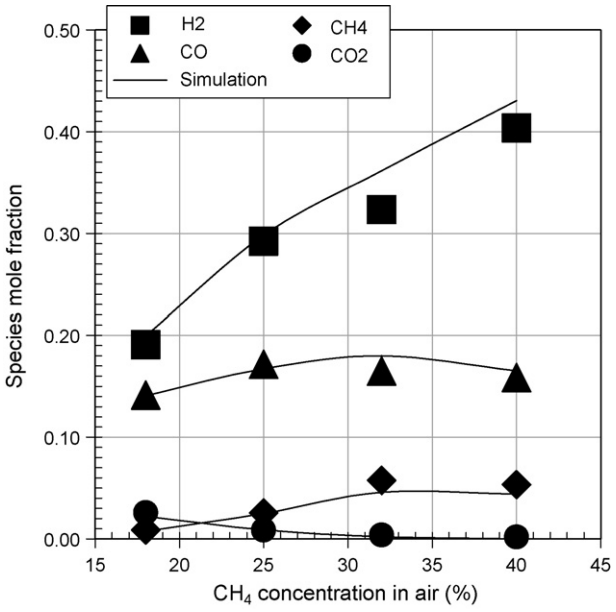

Fig. 4. Experimental (symbols) and numerical (lines) H_2, CO, CO_2 and CH_4 mole fractions *vs.* initial CH_4 concentration in air (mass flow rate = 0.004 g s^{-1}).

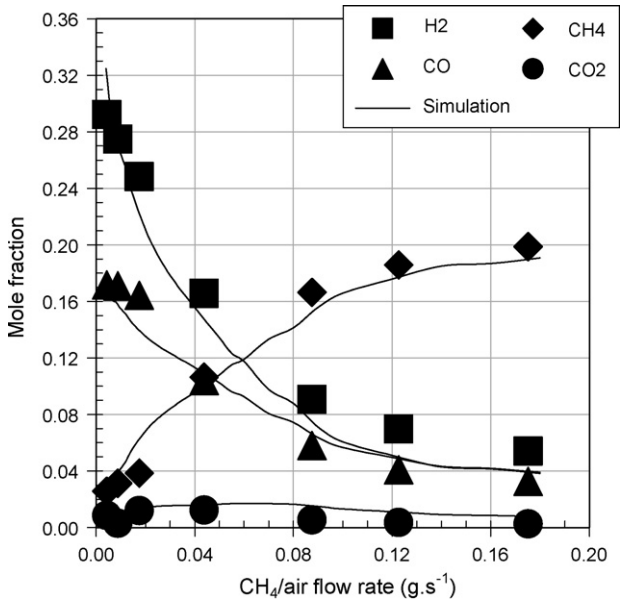

Fig. 5. Experimental (symbols) and numerical (lines) H_2, CO, CO_2 and remaining CH_4 mole fractions *vs.* CH_4/air mass flow rate ($[CH_4]_0 = 25\%$).

Fig. 6 shows electrical power and energy cost of H_2 production as a function of mass flow rate. P_{el} increases from 110 to 155 W and EC_{H_2} decreases from 275 to 50 $kWh/kg_{(H_2)}$ for a mass flow rate increasing from 0.004 to 0.175 $g\,s^{-1}$, respectively.

For the highest total mass flow rate (0.175 $g\,s^{-1}$) studied, the H_2 mole fraction is minimum and P_{el} is maximum (0.05 and 155 W, respectively) corresponding to the lowest EC_{H_2} value (~ 45 $kWh/kg_{(H_2)}$). From these results, it appears that the best energy costs are achieved for the highest mass flow rate studied and are in quite good agreement with those reported in the literature: around 1 $kWh/kg_{(H_2)}$ for plasma technology assisted by catalysis [32], from 1 to 139 $kWh/kg_{(H_2)}$ for gliding arc technology [29,30,33], up to 30 $kWh/kg_{(H_2)}$ for corona discharge technology [34], from 300 to 4000 $kWh/kg_{(H_2)}$ for dielectric barrier discharge technology [35], and from 17 to 1000 $kWh/kg_{(H_2)}$ for conventional technology (autothermal, O_2/air-fired or steam reformer) or electrolytic processes [36–39].

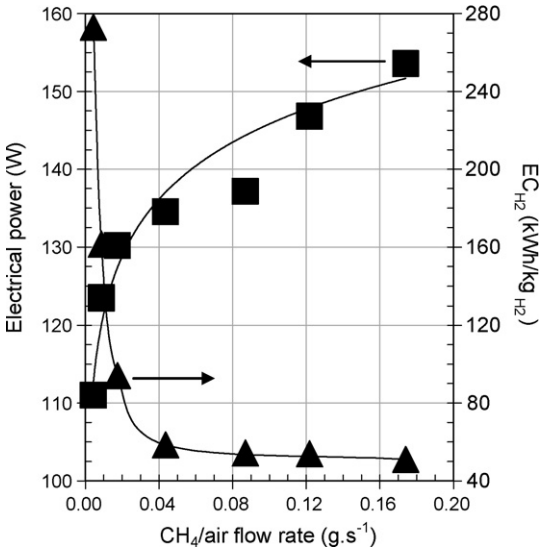

Fig. 6. P_{el} and EC_{H_2} *vs.* mass flow rate ($[CH_4]_0 = 25\%$).

4. Simulation

4.1. Reactor model

Kinetic modeling is a useful tool to study gas phase processes and to gain insight into the chemical mechanisms inside an experimental bulk gas phase. Non-thermal plasma provides energy for active species generation: electrons, ions and free radicals which are involved in the chemical reactions induced. However, modeling with plasma mechanisms describing in detail both chemical kinetics and fluid dynamics is not easily available today. To simulate the experimental methane reforming process by NTP, numerical computations were performed with the following assumptions [15,24,40,41]:

- Thermal decomposition is assumed to be negligible at the inlet of the plasma reactor for initial experimental conditions (295–630 K).
- The discharge effect is considered as an additional energy source to the chemical processes inside the reactor.
- The methane reforming by NTP is described only by the radical behaviour and takes place mainly in the reactive volume ($V \approx 7.1\ cm^3$). Modeling is performed only with a kinetic scheme of the methane oxidation chemistry process in gas phase without the inclusion of specific plasma processes (post-discharge kinetics).
- Radical production is proportional to the related bulk gas composition.
- Radicals and reactants are well mixed and uniformly distributed (*i.e.* 0-D model) within the reactive volume which is assumed to be equivalent to a perfectly stirred reactor (PSR).

Chemical transformation computations, performed with the PSR code [42] from the CHEMKIN-II package [43] and methane reforming chemical kinetics by a non-thermal plasma, are conducted by using the Konnov methane oxidation mechanism [44,45]. Input parameters of the model are:

- constant flow rate (0.004 $g\,s^{-1}$) for $[CH_4]_0$ ranged from 18 to 40%,
- $[CH_4]_0 = 25\%$ at flow rate in the range 0.004–0.175 g/s,
- atmospheric pressure,
- gas temperature at the inlet of the plasma discharge as a function of mass flow rate (480–630 K, see Fig. 2),
- each experimental mole fraction is simulated by numerical fitting of an adjusted negative value of Q (heat inlet through reactor walls corresponds to $Q < 0$) taking into account discharge electrical power, mass flow rate and initial CH_4 concentration.

4.2. Energy balance: experimental and modeling

In the steady state case at constant temperature, the energy conservation equation for a PSR can be written:

$$Q = \dot{m} \cdot \sum_{k=1}^{N} Y_k^* \cdot (h_k^* - h_k) - V \cdot \sum_{k=1}^{N} h_k \cdot W_k \cdot \mu_k \quad (1)$$

The first and second terms of Eq. (1) represent the power exchange due to mass enthalpy variations and mass flow rate (Eq. (2)) and the power exchange due to chemical reactions (Eq. (3)), respectively.

$$P_{fr} = -\dot{m} \cdot \sum_{k=1}^{N} Y_k^* \cdot (h_k^* - h_k) \quad (2)$$

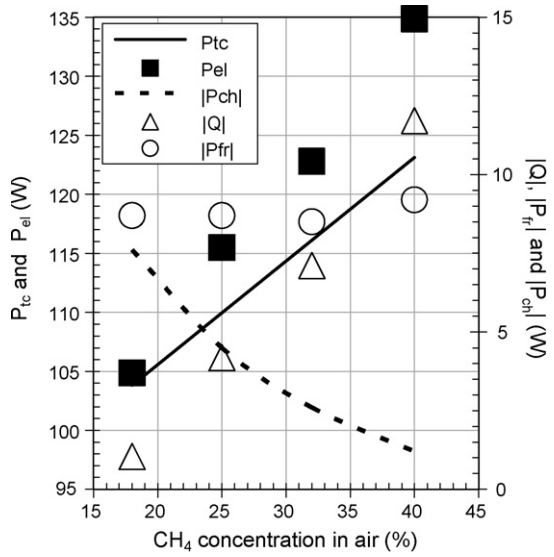

Fig. 7. P_{tc}, P_{el}, $|Q|$, $|P_{fr}|$, $|P_{ch}|$ values *vs.* CH_4 amount (mass flow rate = 0.004 g s^{-1}).

$$P_{ch} = -V \cdot \sum_{k=1}^{N} h_k \cdot W_k \cdot \mu_k \quad (3)$$

The energy balance is the sum of various contributions:

- electrical power corresponding to Joule heating of the plasma column (P_{el}),
- heat power losses or thermal conduction exchanges at high flow rates (P_{tc}),
- power exchange due to flow rate with enthalpy variations per unit of mass (P_{fr}),
- power exchange due to chemical reactions (P_{ch}).

By neglecting radiation losses in the case of electrical discharge, the energy balance can be written by the following expression:

$$P_{el} - P_{tc} - P_{fr} + P_{ch} = 0 \quad (4)$$

From Eqs. (1)–(4), Q can be written as follows:

$$Q = P_{tc} - P_{el} \quad (5)$$

5. Numerical results and discussion

5.1. CH_4 concentration effect on exhaust gas concentration

The calculated outlet species mole fractions obtained by using the above PSR model and the heat exchange power (Q) as fitting parameter are compared to experimental data. Taking into account the calculated species' concentrations and Q value, both P_{ch} and P_{fr} can also be calculated. Experimental (symbols) and numerical (line) species mole fractions are shown as a function of initial CH_4 concentration in air in Fig. 4. For $[CH_4]_0$ in the range 18–40%, good agreement (within 5–10%) is observed between the computed H_2, CO, CO_2 and CH_4 mole fractions and experiments.

In Fig. 7, the computed values of $|Q|$, $|P_{ch}|$, $|P_{fr}|$ and P_{tc} and the experimental values of P_{el} are plotted as a function of CH_4 amount. When $[CH_4]_0$ increases from 18 to 40%, the values of heat exchanges $|Q|$ increase from 1 to 12 W. This increase in $|Q|$ value (linked to the initial increase in CH_4 amount) leads to an increase in power exchange values (P_{tc} from 105 to 125 W, or $|P_{fr}|$ from 8 to 9 W). $|P_{ch}|$ decreases from 8 to 1 W and P_{el} increases from 105 to 135 W. From Fig. 7, it can be seen that $|P_{ch}|$ represents only 1–8% of P_{el}. Thus, only a small part of the electrical energy supplied is involved in partial oxidation of methane. So, when the CH_4 amount increases, a major part of the discharge energy, corresponding to P_{el}, is lost by heat transfer and thermal conduction exchanges, P_{tc} and $|P_{fr}|$, respectively. These results show that the highest power efficiency to convert methane (higher $|P_{ch}|$ and lower P_{tc} or $|P_{fr}|$ values) into syngas is observed for low $[CH_4]_0$.

In the whole range of CH_4 amount, the assumptions chosen ($|Q|$ in the range 1–12 W and PSR configuration) to simulate CH_4/air treatment by a non-thermal plasma are fully satisfactory. The CH_4 oxidation kinetic model of Konnov can describe H_2, CO, CO_2 and CH_4 species mole fractions with a relatively good precision (within 5–10%). Thus, only a small part of the electrical energy supplied contributes to the chemical reaction and most of this electrical energy is involved in thermal losses.

5.2. Mass flow rate effect at outlet gas concentration

Comparison between experimental (symbols) and numerical (line) data as a function of CH_4/air mass flow rate is shown in Fig. 5 at a given $[CH_4]_0$ (25%). Numerical mole fractions are in good agreement (±5%) with experimental data for a mass flow rate below 0.08 g s^{-1} and a relative difference in the range 5–20% is observed for a mass flow rate equal to or higher than 0.08 g s^{-1}.

The computed values of $|Q|$, $|P_{ch}|$, $|P_{fr}|$ and P_{tc} and the experimental values of P_{el} as a function of CH_4/air mass flow rate are plotted in Fig. 8. A linear variation of P_{fr} (10–270 W) is observed in the full range of mass flow rate. Fig. 8 shows two domains for $|Q|$ variations: a first one with a constant variation of $|Q|$ (value around 10 W) and a second one with a linear increase in $|Q|$ from 10 to 130 W. These fitted values of $|Q|$ are linked to two experimental device domains of mass flow rate:

- up to 0.08 g s^{-1}, with significant thermal conduction effects or power losses (P_{tc}) ranging from 100 to 120 W, corresponding to a significant variation in $|P_{ch}|$ which increases from 5 to 100 W,
- beyond 0.08 g s^{-1}, with a better use of electrical power due to an effect on P_{tc} value decreasing from 120 to 20 W, corresponding to a slight variation in $|P_{ch}|$ which increases less significantly (from 100 to 120 W) than previously.

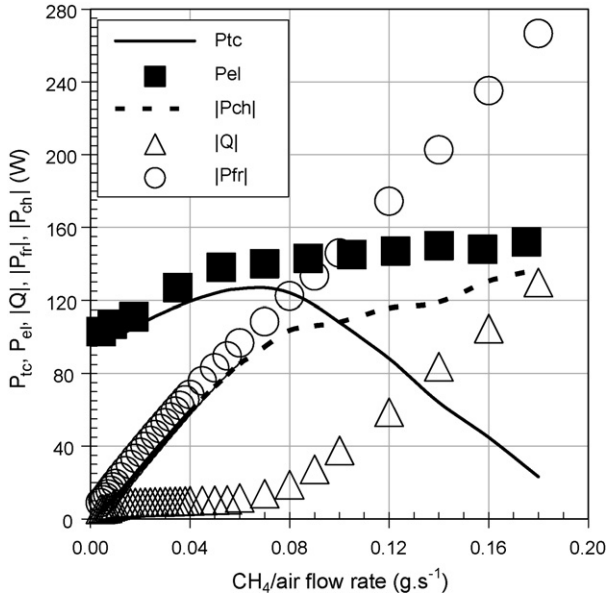

Fig. 8. P_{tc}, P_{el}, $|Q|$, $|P_{fr}|$, $|P_{ch}|$ values *vs.* CH_4/Air mass flow rate ($[CH_4]_0$ = 25%).

For low mass flow rates, the mean plasma discharge power, P_{el}, increases from 100 to 150 W. For a high flow rate, P_{el} is of the same order of magnitude as the chemical power, and losses by thermal conduction are reduced in comparison with data obtained at low flow rates.

At a low mass flow rate, the assumptions chosen ($|Q|$ in the range 5–20 W and a perfectly stirred reactor configuration) to simulate CH_4/air treatment by NTP are fully satisfactory. Indeed, the agreement between experimental and numerical data is within 5–10%. As seen previously, only a small part of the electrical energy supplied is involved in chemical reaction (low $|P_{ch}|$ value) due to high heat transfer and thermal conduction exchanges, P_{tc} and $|P_{fr}|$, respectively. Conversely, for a high mass flow rate (with $|Q|$ in the range 20–130 W), the results are less satisfactory, though still acceptable (agreement within 5–20% between experimental and numerical results). This slight difference could be explained by a non-uniform species distribution within the reaction zone volume due to plasma instabilities and by a small CH_4 conversion rate due to a low residence time. The relative depletion of thermal losses in comparison with the electrical energy supplied to the plasma leads to a better energy efficiency of the device to reform the initial mixture (higher $|P_{ch}|$ value than previously).

6. Conclusion

Experimental investigations of a methane–air mixture injected at atmospheric pressure and ambient temperature in a laboratory-scale non-thermal plasma reactor, as well as the chemical analysis of the main gas products (H_2, CO, CO_2 and unburned CH_4) have been carried out. Maximum H_2 and CO mole fractions in exhaust gas are obtained at a high methane concentration in air (*i.e.* 40%) and low CH_4/air mixture flow rate (*i.e.* 0.004 g s^{-1}). The experimental mean power supplied to the electrical discharge is measured in the range 100–160 W as a function of mass flow rate and CH_4 amount in air. Furthermore, the energy cost can be computed from the mean electrical power and the hydrogen mass flow rate. The best energy cost of H_2 production ($\sim$ 45 kWh/$kg_{(H_2)}$) is observed for the highest CH_4/air mixture mass flow rate.

A kinetic approach to CH_4 reforming by a non-thermal plasma has also been performed using Konnov's oxidation model, initially developed for combustion studies, with assumptions about initial conditions: well-stirred species, gas phase reaction (without specific plasma processes), 0-D model and plasma energy input. Numerical results obtained without any adjustments of the kinetic reactions fit the experimental data rather well, as in all cases, the agreement is within 5–10%. Simulation and experimental data show two main results:

- High CH_4 conversion and maximum H_2 production are obtained at low flow rate and high initial concentration of methane in air. In these cases, most of the electrical energy supplied to the plasma is lost by thermal effect and not involved in the chemical reaction, entailing a high energy cost to produce H_2.
- A low energy cost of H_2 production can be obtained at high flow rates and low initial concentration of methane in air, which decreases losses and enables a better use of electrical power by the chemical reactions.

This study has demonstrated that PSR is a powerful tool for the simulation of gas phase behaviour in methane reforming by a NTP reactor. However, further studies are needed in applying PSR in other experimental conditions, initial fuel or plasma reactors. The technical improvement of such a laboratory-scale reactor needs to be performed with a view to industrial applications: this can be done by considering previous experimental results obtained with gliding discharges [14,15]. Further experiments (*e.g.* in situ spectroscopic diagnostics) can be performed with this NTP reactor to improve the chemical understanding of active species behaviour in the discharge.

References

[1] F. Auprêtre, C. Descorme, D. Duprez, Bio-ethanol catalytic steam reforming over supported metal catalysts, Catal. Commun. 3 (2002) 263–267.
[2] G.A. Deluga, J.R. Salge, L.D. Schmidt, X.E. Verykios, Renewable hydrogen from ethanol by autothermal reforming, Science 303 (2004) 993–997.
[3] J. Llorca, N. Homs, J. Sales, P. Ramirez de la Piscina, Ramirez de la Piscina, efficient production of hydrogen over supported cobalt catalysts from ethanol steam reforming, J. Catal. 209 (2002) 306–317.
[4] J.P. Breen, R. Burch, H.M. Coleman, Metal-catalysed steam reforming of ethanol in the production of hydrogen for fuel cell applications, Appl. Catal. B: Environ. 39 (2002) 65–74.
[5] F.J. Marino, E.G. Cerrella, S. Duhalde, M. Jobbagy, M.A. Laborde, Hydrogen from steam reforming of ethanol. Characterization and performance of copper-nickel supported catalysts, Int. J. Hyd. Energy 23 (12) (1998) 1095–1101.
[6] E.Y. Garcia, M.A. Laborde, Hydrogen production by the steam reforming of ethanol: thermodynamic analysis, Int. J. Hyd. Energy 16 (5) (1991) 307–312.
[7] O. Mutaf-Yardimci, A.V. Saveliev, A.A. Fridman, L.A. Kennedy, Employing plasma as catalyst in hydrogen production, Int. J. Hyd. Energy 23 (12) (1998) 1109–1111.
[8] A. Huang, G. Xia, J. Wang, S.L. Suib, Y. Hayashi, H. Matsumoto, CO_2 reforming of CH_4 by atmospheric pressure ac discharge plasmas, J. Catal. 189 (2000) 349–359.
[9] S. Futamura, H. Kabashima, G. Annadurai, Roles of CO_2 and H_2O as oxidants in the plasma reforming of aliphatic hydrocarbons, Catal. Today 115 (2006) 211–216.
[10] H. Sekiguchi, Y. Mori, Steam plasma reforming using microwave discharge, Thin Solid Films 435 (1/2) (2003) 44–48.
[11] T. Paulmier, L. Fulcheri, Use of non-thermal plasma for hydrocarbon reforming, Chem. Eng. J. 106 (2005) 59–71.
[12] A. Czernichowski, GlidArc assisted preparation of the synthesis gas from natural and waste hydrocarbons gases, oil & gas science and technology, Rev. IFP 56 (2) (2001) 181–198.
[13] M.G. Sobacchi, A.V. Saveliev, A.A. Fridman, L.A. Kennedy, S. Ahmed, T. Krause, Experimental assessment of a combined plasma/catalytic system for hydrogen production via partial oxidation of hydrocarbon fuels, Int. J. Hyd. Energy 27 (6) (2002) 635–642.
[14] J.D. Rollier, J. Gonzalez-Aguilar, G. Petitpas, A. Darmon, L. Fulcheri, R. Metkemeijer, Experimental study on gasoline reforming assisted by nonthermal arc discharge, Energy Fuels 22 (2008) 556–560.
[15] A. Indarto, J.W. Choi, H. Lee, H.K. Song, Kinetic modeling of plasma methane conversion using gliding arc, J. Nat. Gas Chem. 14 (2005) 13–21.
[16] L.M. Zhou, B. Xue, U. Kogelschatz, B. Eliasson, Nonequilibrium plasma reforming of greenhouse gases to synthesis gas, Energy Fuels 12 (1998) 1191–1199.
[17] H.D. Gesser, N.R. Hunter, D. Probawono, The CO_2 reforming of natural gas in a silent discharge reactor, Plasma Chem. Plasma Process. 18 (2) (1998) 241–245.
[18] K. Supat, A. Kruapong, S. Chavadej, L.L. Lobban, R.G. Mallinson, Synthesis gas production from partial oxidation of methane with air in AC electric gas discharge, Energy Fuels 17 (2003) 474–481.
[19] J.M. Cormier, I. Rusu, Syngas production via methane steam reforming with oxygen: plasma reactors versus chemical reactors, J. Phys. D: Appl. Phys. 34 (2001) 2798–2803.
[20] L. Bromberg, D.R. Cohn, A. Rabinovich, J.E. Surma, J. Virden, Compact plasmatron-boosted hydrogen generation technology for vehicular applications, Int. J. Hyd. Energy 24 (1999) 341–350.
[21] L. Bromberg, D.R. Cohn, A. Rabinovich, J. Heywood, Emissions reductions using hydrogen from plasmatron fuel converters, Int. J. Hyd. Energy 26 (2001) 1115–1121.
[22] G. Petitpas, J.D. Rollier, A. Darmon, J. Gonzalez-Aguilar, R. Metkemeijer, L. Fulcheri, Acomparative study of non-thermal plasma assisted reforming technologies, Int. J. Hyd. Energy 32 (2007) 2848–2867.
[23] O. Aubry, C. Met, A. Khacef, J.M. Cormier, On the use of a non-thermal plasma reactor for ethanol steam reforming, Chem. Eng. J. 106 (2005) 241–247.
[24] M.S. Benilov, G.V. Naidis, Modeling of hydrogen-rich gas production by plasma reforming of hydrocarbon fuels, Int. J. Hyd. Energy 31 (2006) 769–774.
[25] S. Kado, K. Urasaki, Y. Sekine, K. Fujimoto, Direct conversion of methane to acetylene or syngas at room temperature using non-equilibrium pulsed discharge, Fuel 82 (2003) 1377–1385.
[26] Y.P. Zhang, Y. Li, Y. Wang, C.J. Liu, B. Eliasson, Plasma methane conversion in the presence of carbon dioxide using dielectric-barrier discharges, Fuel Process. Technol. 83 (2003) 101–109.
[27] C.J. Liu, B. Xue, B. Eliasson, F. He, Y. Li, G.H. Xu, Methane conversion to higher hydrocarbons in the presence of carbon dioxide using dielectric-barrier discharge plasmas, Plasma Chem. Plasma Process. 21 (2001) 301–310.

[28] I. Rusu, J.M. Cormier, On a possible mechanism of the methane steam reforming in a gliding arc reactor, Chem. Eng. J. 91 (2003) 23–31.
[29] E. El Ahmar, C. Met, O. Aubry, A. Khacef, J.M. Cormier, Hydrogen enrichment of a methane–air mixture by atmospheric pressure plasma for vehicle applications, Chem. Eng. J. 116 (2006) 13–18.
[30] F. Ouni, Production d'hydrogène et valorisation des alcanes par plasma non thermique, PhD Thesis, Université d'Orléans, GREMI, 2006.
[31] H. Nassar, S. Pellerin, K. Musiol, O. Martinie, N Pellerin and J-M Cormier, $N^+{}_2/N_2$ ratio and temperature measurements based on the first negative $N^+{}_2$ and second positive N_2 overlapped molecular emission spectra, J. Phys. D: Appl. Phys. 37 (2004) 1904–1916.
[32] Y. Chao, C.T. Huang, H.M. Lee, M.B. Chang, Hydrogen production via partial oxidation of methane with plasma-assisted catalysis, Int. J. Hyd. Energy 33 (2) (2008) 664–671.
[33] D.H. Lee, K.T. Kim, M.S. Cha, Y.H. Song, Optimization scheme of a rotating gliding arc reactor for partial oxidation of methane, in: Proceedings of the Combustion Institute, vol. 31, 2007, pp. 3343–3351.
[34] G.B. Zhao, S. John, J.J. Zhang, L. Wang, S. Muknahallipatna, J.C. Hamann, J.F. Ackerman, M.D. Argyle, O.A. Plum, Methane conversion in pulsed corona discharge reactors, Chem. Eng. J. 125 (2006) 67–79.
[35] B. Sarmiento, J.J. Brey, I.G. Viera, A.R. Gonzalez-Elipe, J. Cotrino, V.J. Rico, Hydrogen production by reforming of hydrocarbons and alcohols in a dielectric barrier discharge, J. Power Sources 169 (2007) 140–143.
[36] N. Muradov, F. Smith, A. T-Raissi, Hydrogen production by catalytic processing of renewable methane-rich gases, Int. J. Hyd. Energy 33 (2008) 2023–2035.
[37] C.E. Thomas, I.F. Kuhn Jr., B.D. James, F.D. Lomax Jr., G.N. Baum, Affordable hydrogen supply pathways for fuel cell vehicles, Int. J. Hyd. Energy 23 (6) (1998) 507–516.
[38] C.E. Thomas, B.D. James, F.D. Lomax Jr., I.F. Kuhn Jr., Fuel options for the fuel cell vehicle: hydrogen, methanol or gasoline? Int. J. Hyd. Energy 25 (2000) 551–567.
[39] M. Jasinski, M. Dors, J. Mizeraczyk, Production of hydrogen via methane reforming using atmospheric pressure microwave plasma, J. Power Sources 181 (2008) 41–45.
[40] S.A. Nair, T. Nozaki, K. Okazaki, Methane oxidative conversion pathways in a dielectric barrier discharge reactor-investigation of gas phase mechanism, Chem. Eng. J. 132 (2007) 85–95.
[41] A. Indarto, J.-W. Choi, H. Lee, H.K. Song, Methane conversion using dielectric barrier discharge: comparison with thermal process and catalyst effects, J. Nat. Gas Chem. 15 (2006) 87–92.
[42] P. Glarborg, R.J. Kee, J.F. Grcar, J.A. Miller, PSR: A FORTRAN program for modeling well-stirred reactors, Sandia Report SAND86-8209, 1986.
[43] R.J. Kee, F.M. Rupley, J.A. Miller, CHEMKIN-II: A fortran chemical kinetics package for the analysis of gas-phase chemical kinetics, Sandia Report SAND89-8009, 1989.
[44] A.A. Konnov, Detailed reaction mechanism for small hydrocarbons combustion, Release 0.5 http://homepages.vub.ac.be/∼akonnov/, 2000 (accessed August 2008).
[45] A.A. Konnov, Development and validation of a detailed reaction mechanism for the combustion of small hydrocarbons, Proceedings of the Combustion Institute 28 (2000) 317.